13 Phase Transitions and Superconducting Photon Detectors

A. Gazizulina, S. Huangfu, A. Schilling, S. Siegrist, Q. Wang and X. Zhang

in collaboration with: University of Bern (K. Krämer), Deutsches Zentrum für Luft- und Raumfahrt (Prof. Alexei Semenov), Paul-Scherrer Institut (Dr. Marisa Medarde), Paul-Scherrer Institut (Prof. Kazimierz Conder), McMaster University (Dr Hanna Dabkowska), Max Planck Institute for Chemical Physics and Solids, Dresden (Prof. C. Felser), Universidad del Pais Vasco (Prof. Evgeny Sherman), Academy of Sciences of Uzbekistan (Prof. Abdulla Rakhimov), Leibniz-Institut für Festkörper- und Werkstoffforschung (IFW) (Dr. Vladimir Kataev), Helmholtz Research Centre Dresden-Rossendorf (Dr. Tobias Förster), Radboud University Nijmegen (Dr. Laurens Peters), Universitetet i Stavanger (Prof. Diana Quintero Castro), Helmholtz Zentrum für Materialien und Energie HZB (Dr. Illya Glavatskyy), Laboratoire National des Champs Magnetiques Intenses (lmcmi) (Dr. Albin De Muer), Deutsches Zentrum für Luft- und Raumfahrt (Dr. Heinz-Wilhelm Hübers), Karlsruhe Institut für Technologie (Dr. Konstantin Ilín)

13.1 Superconducting nanowire single photon detectors (SNSPD)

13.1.1 Detection mechanisms

All of the currently proposed detection mechanisms for SNSPDs are based on a photon induced non-equilibrium area, namely a hotspot, playing an important role in most SNSPDs. The different detection models predict different hotspot sizes depending on the superconducting material, but they are unable to explain all the experimental results so far. By measuring the inelastic interaction time, electron diffusion constant, and quasiparticle lifetime, we defined the hotspot size more precisely [1]. With this definition, we can explain all the current phenomena in SNSPDs, for instance, the temperature, current and wavelength dependences of the detection efficiency. The definition of the hotspot size has also been experimentally confirmed by a two-photon delay experiment [2].

WSi has become the most fascinating material for SNSPDs, which holds the record of detection efficiency (up to $\approx$ 93%) [3]. The underlying mechanism responsible for the good performance of this promising material, however, is still unknown. We successfully deposited ultrathin amorphous WSi films with critical temperatures T_c comparable to and even higher than those used by other groups, as it is shown in Fig. 13.1. In order to figure out the mechanism of the high detection efficiency for WSi-based SNSPDs, we measured the superconducting material parameters through magneto-transport experiments [1]. We found that the superconducting coherence length in this amorphous material is larger than that in crystalline or granular NbN materials. Therefore, detectors based on this material are more robust to electrical and geometrical constrictions. As a result, the experimental critical current is closer to the local depairing current, and the detection efficiency becomes very high. The most striking characteristics of WSi are the long electron-phonon interaction time and intrinsic quasiparticles lifetime, as shown in Fig 13.2.

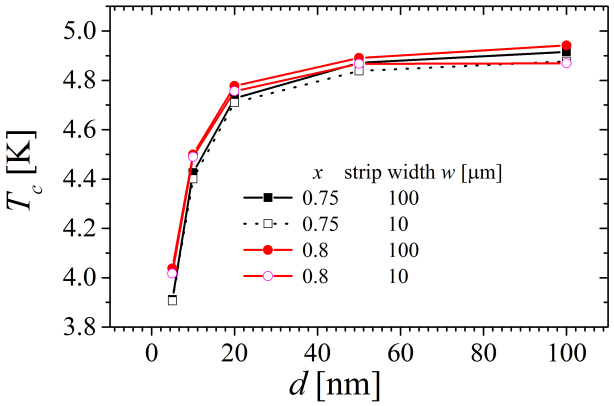

FIG. 13.1 – Critical temperatures of WSi films as a function of the film thickness.

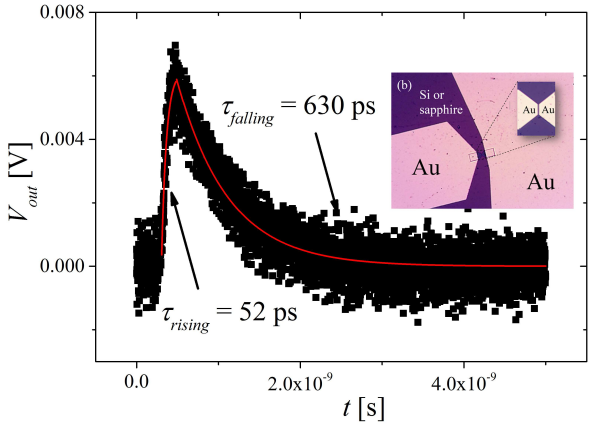

FIG. 13.2 – Measurement of the quasiparticle lifetime in amorphous WSi. Inset: the device used for the measurement [1].

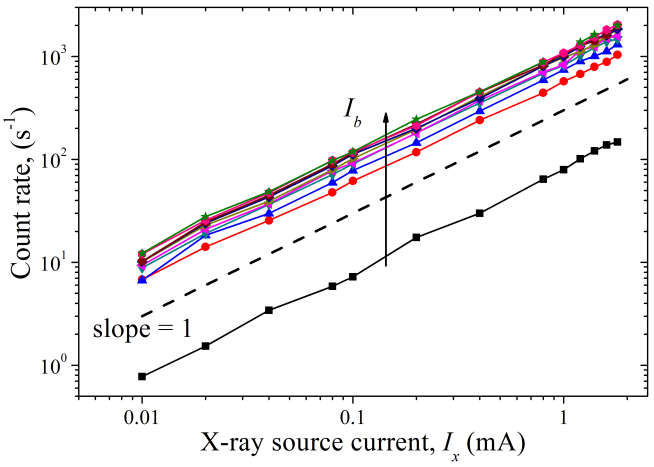

FIG. 13.3 – Measured count rates vs the X-ray source current I_x (with an acceleration voltage V_A = 30 kV) at bias current I_b ranging from 10 μA to 100 μA, with an increment of 10 μA. The dashed line indicates a slope of 1.

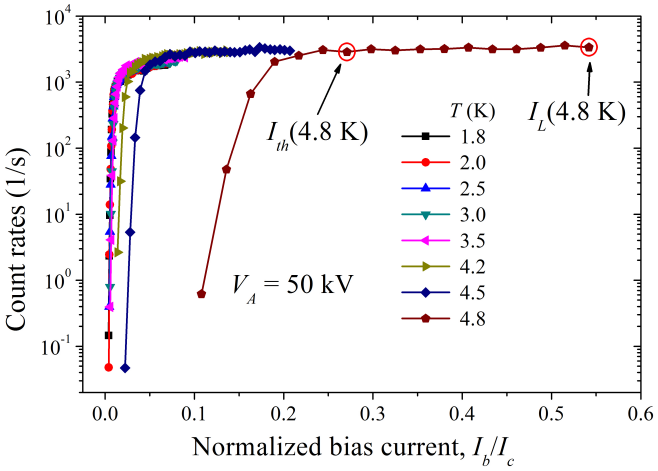

FIG. 13.4 – Count rates as functions of the reduced bias current (normalized to the critical current at each temperature) with an acceleration voltage of 49.9 kV.

The relatively long electron-phonon interaction time suppresses the probability of electron thermalization through the phonon channel, which makes the photon energy conversion efficiency higher in WSi than in other materials. Moreover, a large intrinsic quasiparticle lifetime results in a larger hotspot in WSi. In summary, our models and experimental data successfully explain the remarkable detection efficiency of WSi as compared to NbN.

[1] Zhang X., Engel A., Wang Q., Schilling A., Semenov A., Sidorova M., Hübers H.-W., Charaev I., Ilin K., and Siegel M.,
Rev. B, 94:174509, 2016.

[2] Marsili F., Stevens M. J., Kozorezov A., Verma V. B., Lambert C., Stern J. A., Horansky R. D., Dyer S., Duff S., Pappas D. P., Lita A. E., Shaw M. D., Mirin R. P., and Nam S. W.,
Phys Rev. B, 93:094518, 2016.

[3] Marsili F., Verma V. B., Stern J. A., Harrington S., Lita A. E., Gerrits T., Vayshenker I., Baek B., Shaw M. D., Mirin R. P., and Nam S. W.,
Nature Photonics, 7:210, 2013.

13.1.2 X-ray sensitive superconducting photon detectors

One of our most interesting results in our research on single X-ray photon detectors (X-SNSPD) comes from the amorphous nature of the WSi films [4]. The amorphous structure makes this type of detectors more robust against radiation damage and therefore makes them suitable for detecting high-energy particles. Moreover, due to their modest requirements on substrate quality and deposition conditions, very large and complicated WSi X-SNSPDs can be produced relatively easily on different substrates.

Our WSi X-SNSPDs show no degradation of their superconducting properties after the device fabrication, which is very different from the commonly used NbN based devices. In Fig. 13.3, we illustrate the single X-ray photon resolving ability of a WSi X-SNSPD. The linear slope of the curves indicates that our detector works in the single-photon regime at all bias currents. The detection performance of our detector is shown in Fig. 13.4. A saturated detection efficiency is observed at all temperatures, which ensures a high signal-to-noise ratio. Unlike optical SNSPDs, which need to be operated at ultralow temperature ($T/T_c << 1$) our WSi detector is able to sense X-ray photons up to the critical temperature. Due to the amorphous nature and relatively large magnetic penetration depth, the bias current is very stable within the nanowire, and thermal fluctuations can therefore be ignored. As a consequence, the dark counts in our X-SNSPD are negligible. All these properties, saturated quantum detection efficiency, negligible dark counts and ultrafast response, make our X-SNSPDs competitive to the best ultrafast X-ray photon detectors on the market.

[4] Zhang X., Wang Q., and Schilling A.,
AIP Advances, 6:115104, 2016.

13.2 Insulator-to-metal transition in $CsAuCl_3$ and $CsAuBr_3$

In a series of experiments, we studied the physical properties of $CsAuCl_3$ and $CsAuBr_3$. It is known that $CsAuCl_3$ undergoes an insulator-to-metal transition under the application of external pressure, which is accompanied by a tetragonal-to-cubic phase transition at $p \approx 12.5$ GPa at $T = 300$ K [5]. Corresponding Raman investigations strongly indicate a transition from mixed valent (MV) Au(I)Au(III) to formally single valent (SV) Au(II)Au(II) in the metallic state

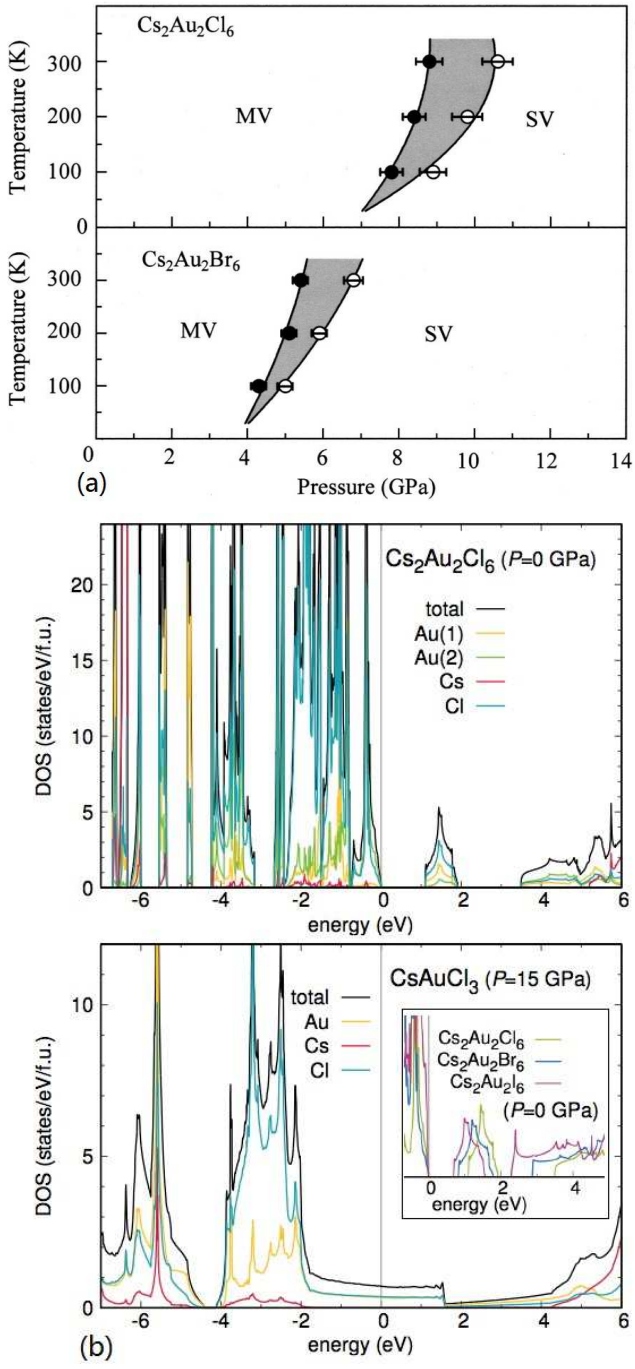

FIG. 13.5 – (a) Mixed valent (MV) to single valent (SV) transition of Au in $CsAuX_3$ with X = Cl and Br (taken from Ref. [6]); (b) Electron density of states (EDOS) of $CsAuCl_3$ for ambient and high pressure. The inset displays the EDOS at ambient pressure for the respective Cl, Br and I variants.

with delocalized charge carriers (see Fig. 13.5(a)) [6]. This situation is very similar to $Ba_{1-x}K_xBiO_3$ [7], in which the substitution of Ba by K not only changes the crystal structure from monoclinic to cubic but also lifts the mixed-valent character of Bi(III)Bi(V) of the insulator $BaBiO_3$, leading to

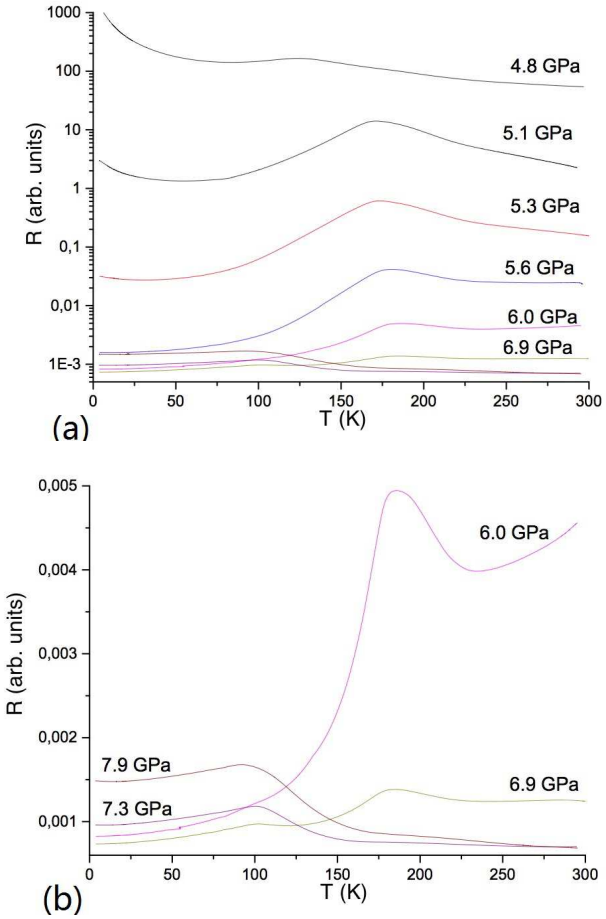

FIG. 13.6 – Evolution of the resistivity of a single crystal of $CsAuBr_3$ under external pressure

a quasi single valent Bi(IV)Bi(IV) state, which is metallic and even superconducting below $T_c \approx 30$ K for $x \approx 0.37$ [7].

In a first step, we wished to obtain more precise information on the electronic structure of these compounds (in collaboration with Prof. R. Thomale, Univ. Würzburg, Germany). Corresponding electronic structure calculations using the full-potential local-orbital minimum-basis scheme confirmed that the high-pressure phase of $CsAuCl_3$ shows a finite density of states at the Fermi level, in contrast to the situation at ambient pressure (see Fig. 13.5(b)). Moreover, at $p = 15$ GPa, the Au(I)-Au(III) character is lost, with a nominal Au(II) valency, but without stabilization of a magnetic moment. The energy gap at ambient pressure is gradually reduced when Cl is replaced by Br or I (see inset of Fig. 13.5(b)).

We have grown single crystals of $CsAuCl_3$ and $CsAuBr_3$ according to the recipe published in Ref. [8]. Inspired by the diagram shown in Fig. 13.5(a), we have measured the resistivity of $CsAuBr_3$ at external pressures up to 7.9 GPa (see Fig. 13.6, in collaboration with Dr. S. Medvedev and Prof. C. Felser, Max Planck Institute for Chemical Physics and Solids, Dresden, Germany). At 4.8 GPa, $CsAuBr_3$ is

semiconducting with some anomaly at ∼130 K. The resistivity decreases several orders of magnitude upon increasing the pressure up to 6-7 GPa (see Fig. 13.6(a)). At pressures above 6 GPa (Fig. 13.6(b)), the evolution of the resistivity is peculiar, with a slight gradual increase at low temperature, with some resemblance to the behaviour of $CsAuI_3$ [9]. There must be various phase transitions (or crossovers) involved, whose origin remains to be investigated.

[5] Matsushita N., Ahsbahs H., Hafner S. S., and Kojima N., Rev. High Pressure Sci. Technol., 7:329, 1998.

[6] Liu X. J., Moritomo Y., Nakamura A., and Kojima N., J. Chem. Phys., 110:9174, 1999.

[7] Cava R. J., Batlogg B., Krajewski J. J., Farrow R., Rupp L. W., Short K., Peck W. F., and Kometani T., Nature, 332:814, 1998.

[8] Riggs S. C., Shapiro M. C., Corredor F., Geballe T. H., Fisher I. R., MAcCandless G. T., and Chan J. Y., J. Crystal Growth, 355:13, 2012.

[9] Kojima N., Fukuhara F., Kitagawa H., Takahashi H., and Mori N., Synthetic Metals, 86:2175, 1997.

13.3 Investigations on the quantum magnets $Sr_3Cr_2O_8$ and $Ba_3Cr_2O_8$

$Sr_3Cr_2O_8$ and $Ba_3Cr_2O_8$ are two insulating dimerized spin systems with the spin 1/2 magnetic ions Cr^{5+}. These ions are located in hexagonal bilayers with a strong antiferromagnetic interaction that leads to a singlet ground state and triplet states separated from the singlet state by an energy gap Δ. This gap closes as soon as the external magnetic field reaches a critical value H_c which is given by the Zeeman splitting of the triplet states. We have previously shown that the intradimer interaction constant J_0 as well as H_c strongly depend on stoichiometry if Ba is successively replaced by Sr ($Ba_{3-x}Sr_xCr_2O_8$), thereby introducing disorder and an expansion of the unit cell [10–12].

[10] Grundmann H., Schilling A., Medarde M., and Sheptyakov D., Physical Review B, 90:075101, 2014.

[11] Grundmann H., Schilling A., Marjerrison C.A., Dabkowska H.A., and Gaulin B.D., Mat. Res. Bull., 48:3108, 2013.

[12] Grundmann H., Gazizulina A., Schilling A., von Rohr F., Forster T., and Peters L., New J. Phys., 18:033001, 2016.

13.3.1 Magnetization measurements on single crystals

Single crystals of $Ba_{3-x}Sr_xCr_2O_8$ were successfully grown for x = 2.8 and 2.9 at the Helmholtz Zentrum Berlin (HZB) by using a high-temperature optical floating-zone furnace (in collaboration with Prof. Bella Lake). In Fig.13.7, we show the magnetic susceptibilities for magnetic fields applied parallel and perpendicular to the c-axes, respectively [13]. The magnetic behaviour is typical for dimerized spin systems, and is in agreement with our previous measurements on polycrystalline samples [11]. However, the data show a certain directional dependence, particularly for x = 2.8, which suggests a weakly anisotropic tensor of the gyromagnetic g factor, as it has been also reported for the pure $Br_3Cr_2O_8$ (x = 0) [14].

[13] Gazizulina A., Quintero-Castro D., and Schilling A., in preparation.

[14] Kofu M., Ueda H., Nojiri H., Oshima Y., Zenmoto T., Rule K. C., Gerischer S., Lake B., Batista C. D., Ueda Y., and Lee S.-H., Physical Review Letters, 102:177204, 2009.

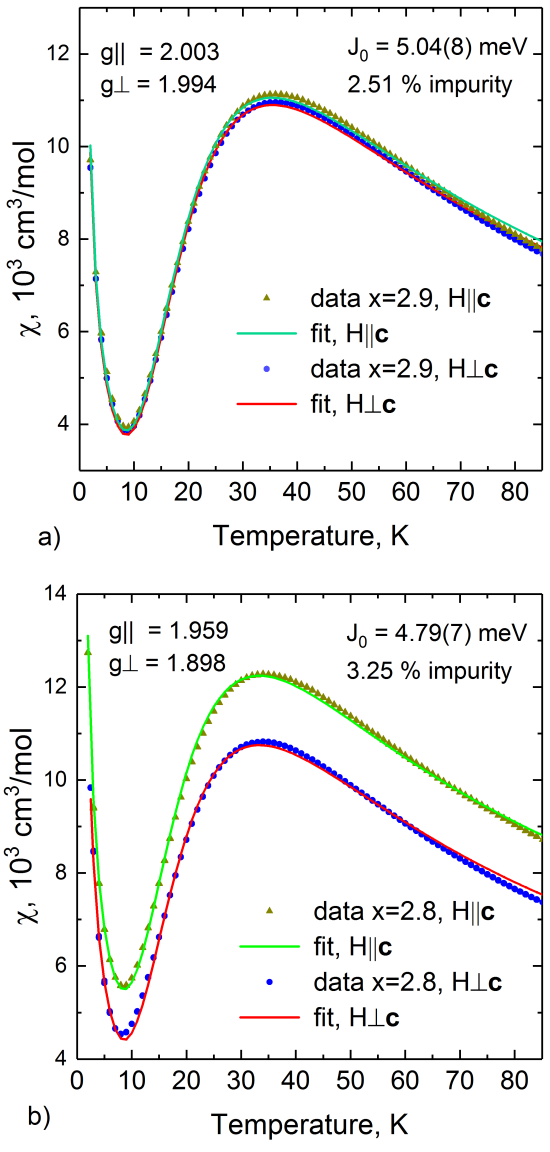

FIG. 13.7 – Magnetic susceptibilities for single crystals of *a*) $Ba_{0.1}Sr_{2.9}Cr_2O_8$ and *b*) $Ba_{0.2}Sr_{2.8}Cr_2O_8$ with magnetic fields parallel and perpendicular to c, respectively.

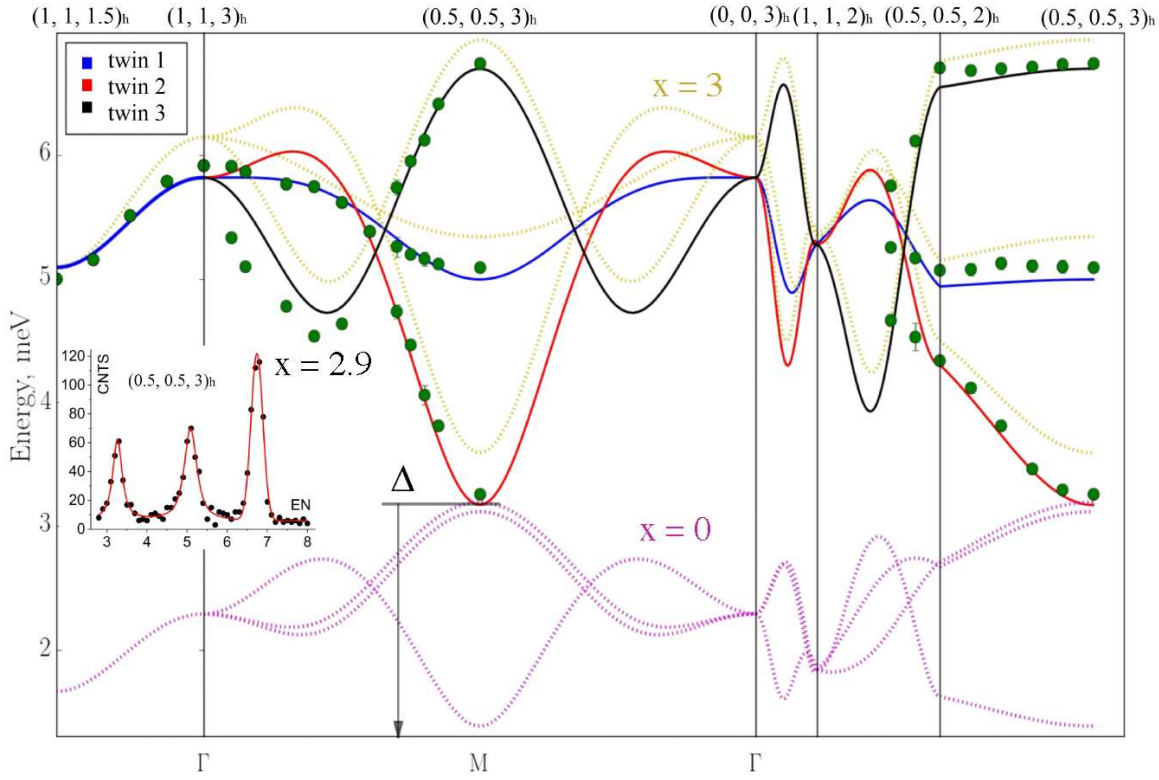

FIG. 13.8 – Measured room-temperature dispersion relation for $Ba_{0.1}Sr_{2.9}Cr_2O_8$ from our inelastic neutron scattering experiments [15]. The solid lines correspond to a random-phase approximation model for three different Jahn-Teller induced crystal domains, rotated 60° with respect to each other. The calculated relations for $Sr_3Cr_2O_8$ (x = 3) and $Ba_3Cr_2O_8$ (x = 0) are shown for comparison.

13.4 Magnetic dispersion relation in $Ba_{0.1}Sr_{2.9}Cr_2O_8$

To complement our investigations on $Ba_{3-x}Sr_xCr_2O_8$, we have performed a series of inelastic neutron scattering measurements (at HZB Berlin, Germany), to directly measure the magnetic coupling constants and the spin gap Δ [15]. In Fig.13.8, we show our corresponding data that we obtained on a $Ba_{0.1}Sr_{2.9}Cr_2O_8$ single crystal, and we fitted them with a random-phase approximation model similar to that described in Ref. [16] for $Sr_3Cr_2O_8$. To achieve this, we had to respect the fact that due to a Jahn-Teller distortion (see our last annual report), three different crystal twin domains, rotated by 60° with respect to each other, have to be taken into account, resulting in three dispersion modes that merge in the center of the Brioullin zone (i.e., in the Γ point). The result for the intradimer interaction constant J_0 is consistent with our previously published results [17–19]. The spin gap Δ (i.e., the minimum in the dispersion relation) is at Δ = 3.23 meV (see Fig. 13.8) resulting in a critical field $\mu_0 H_c = \Delta/g\mu_B \approx 28.8$ T (using $g = 2$), which compares favourably with our published value $\mu_0 H_c \approx 28.6(1)$ T from our high-field magnetization measurements [19]. The corresponding value for pure $Sr_3Cr_2O_8$ is $\mu_0 H_c \approx 30.4$ T [16,18].

[15] Gazizulina A., Quintero-Castro D., and Schilling A. in preparation.

[16] Quintero-Castro D. L., Lake B., Wheeler E. M., Islam A.T.M.N., Guidi T., Rule K. C., Izaola Z., Russina M., Kiefer K., Skourski Y., and Herrmannsdorfer T., Physical Review B, 81:014415, 2010.

[17] Grundmann H., Schilling A., Medarde M., and Sheptyakov D., Physical Review B, 90:075101, 2014.

[18] Grundmann H., Schilling A., Marjerrison C.A., Dabkowska H.A., and Gaulin B.D.m Mat. Res. Bull., 48:3108, 2013.

[19] Grundmann H., Gazizulina A., Schilling A., von Rohr F., Forster T., and Peters L.m New J. Phys., 18:033001, 2016.